

# Simulations of complex electron paramagnetic resonance spectra for radiation-induced defect centres in advanced ceramic breeder pebbles

Arturs Zarins<sup>a,b,\*</sup>, Andris Antuzevics<sup>c,d</sup>, Gunta Kizane<sup>a</sup>, Julia M. Leys<sup>e</sup>, Regina Knitter<sup>e</sup>

<sup>a</sup> University of Latvia, Institute of Chemical Physics, 1 Jelgavas Street, LV-1004 Riga, Latvia

<sup>b</sup> Daugavpils University, Faculty of Natural Sciences and Mathematics, 1A Parades Street, LV-5401 Daugavpils, Latvia

<sup>c</sup> University of Latvia, Institute of Solid State Physics, 8 Kengaraga Street, LV-1063 Riga, Latvia

<sup>d</sup> Vilnius University, Institute of Chemistry, 24 Naugarduko Street, 03225 Vilnius, Lithuania

<sup>e</sup> Karlsruhe Institute of Technology, Institute for Applied Materials, 76021 Karlsruhe, Germany

## ARTICLE INFO

### Keywords:

Advanced ceramic breeder pebbles  
Tritium breeding  
Paramagnetic radiation-induced defect centres  
Electron paramagnetic resonance  
Spectra simulation

## ABSTRACT

Advanced ceramic breeder (ACB) pebbles consisting of lithium orthosilicate ( $\text{Li}_4\text{SiO}_4$ ) and the strengthening phase lithium metatitanate ( $\text{Li}_2\text{TiO}_3$ ) are accepted as the European Union's reference solid-state material for tritium breeding in thermonuclear fusion reactors. Previously, the influence of various radiation types on  $\text{Li}_4\text{SiO}_4$ -based ceramic breeder materials has already been investigated and described by several groups of researchers. Electron paramagnetic resonance (EPR) spectroscopy is one of the most frequently used analytical and non-destructive techniques that can be selectively applied for qualitative and quantitative research of radiation-induced defect centres with paramagnetic properties (electron spin  $S \neq 0$ ). In the present work, individual signals of paramagnetic radiation-induced defect centres in the ACB pebbles after irradiation with X-rays were separated by EPR spectra simulations for the first time. Multiple signals of spin  $S = \frac{1}{2}$  systems with distinctive symmetries and g-factor ( $g$ ) values were identified and characterised. Individual signal decay at room temperature was monitored and isochronal annealing of the irradiated ACB pebbles was performed in order to evaluate the stability of accumulated radiation-induced defect centres. Based on the obtained results, it was determined that radiation-induced defect centres with EPR signals in the  $g > 2.00$  region are similar to irradiated single-phase  $\text{Li}_4\text{SiO}_4$  ceramic materials, while additions of  $\text{Li}_2\text{TiO}_3$  as the second phase in the ACB pebbles also stimulates the formation of several titanium-related electron centres with signals in the  $g < 2.00$  region and different thermal properties.

## 1. Introduction

In ITER (International Thermonuclear Experimental Reactor), which is currently under construction at Cadarache, France, several designs of DEMO (Demonstration Power Plant) relevant Test Blanket Modules (TBMs) will be tested in order to verify and compare the developed solid and liquid tritium breeding concepts under real operational conditions of a thermonuclear fusion reactor [1]. Advanced ceramic breeder (ACB) pebbles consisting of lithium orthosilicate ( $\text{Li}_4\text{SiO}_4$ ) and the strengthening phase lithium metatitanate ( $\text{Li}_2\text{TiO}_3$ ) were first suggested by Knitter et al. [2] as a potential solid-state candidate material for tritium breeding in the European Union's (EU) developed Helium Cooled Pebble Bed (HCPB) TBM concept. A composition of 65 mol%  $\text{Li}_4\text{SiO}_4$  and 35 mol %  $\text{Li}_2\text{TiO}_3$  is proposed as an optimal crystalline phase content for the

ACB pebbles [3]. In the past decade, lithium density [4], tritium breeding ratio (TBR) [5], mechanical stability [6], melting point [7], long-term thermal stability [8], tritium release temperature range [9], neutron activation behaviour [10], radiation stability [11], and chemical compatibility with EUROFER97 steel [12] have been investigated for the ACB pebbles and directly compared to the former EU reference ceramic breeder material, i.e.,  $\text{Li}_4\text{SiO}_4$  pebbles produced with a 2.5 wt% surplus of silicon dioxide ( $\text{SiO}_2$ ).

Electron paramagnetic resonance (EPR) spectroscopy is an indispensable tool for the characterisation of radiation-induced defect centres with paramagnetic properties (electron spin  $S \neq 0$ ) in irradiated solid-state materials [13]. The absolute sensitivity of conventional EPR spectrometers reaches  $10^9$  spins, allowing the detection of minuscule amounts of paramagnetic radiation-induced defect centres. EPR has

\* Corresponding author at: University of Latvia, Institute of Chemical Physics, 1 Jelgavas Street, LV-1004 Riga, Latvia.

E-mail address: [arturs.zarins@lu.lv](mailto:arturs.zarins@lu.lv) (A. Zarins).

<https://doi.org/10.1016/j.nme.2023.101458>

Received 16 February 2023; Received in revised form 31 May 2023; Accepted 1 June 2023

Available online 3 June 2023

2352-1791/© 2023 The Authors. Published by Elsevier Ltd. This is an open access article under the CC BY license (<http://creativecommons.org/licenses/by/4.0/>).

already been successfully applied in several investigations to analyse both, type and concentration of paramagnetic radiation-induced defect centres in  $\text{Li}_4\text{SiO}_4$  pebbles produced with a surplus of  $\text{SiO}_2$  after irradiation with X-rays [14], accelerated electrons [15], and neutrons [16]. The line-shape, g-factor ( $g$ ) values, and peak-to-peak linewidth ( $\Delta B_{pp}$ ) have been used as main comparative parameters in order to identify possible origins of the detected EPR signals. Regardless of the type, mass, and energy of radiation, similar EPR signals in the  $g > 2.00$  region have been reported. Recently, from the detailed analysis of EPR spectra annealing behaviour, at least seven  $S = \frac{1}{2}$  systems with distinct thermal stabilities have been identified and characterised [17]. The introduction of  $\text{Li}_2\text{TiO}_3$  as a second phase significantly impacts the formation of paramagnetic radiation-induced defect centres in the ACB pebbles, which is evidenced by the emergence of additional broad and overlapping EPR signals in the  $g < 2.00$  region [18]. However, a detailed analysis deconvoluting these signals into individual components and determining the spin-Hamiltonian (SH) parameters has not been provided so far. Recently, the first *in-situ* tritium release measurements for the ACB pebbles under neutron irradiation conditions have been performed [19]. Therefore, the SH parameters will be indispensable in the near future for reliable identification and local structure assignments of radiation-induced defect centres in the neutron-irradiated ACB pebbles.

In the present work, EPR spectroscopy was used to separate individual signals of paramagnetic radiation-induced defect centres in the ACB pebbles after irradiation with X-rays by EPR spectra simulations for the first time. The exposure to X-rays was selected due to feasibility of performing the EPR spectra measurements immediately after irradiation. The stability of accumulated radiation-induced defect centres in the irradiated pebbles was evaluated by monitoring individual signal decay both at room temperature and after isochronal annealing.

## 2. Experimental

The ACB pebbles (diameter: 500–1000  $\mu\text{m}$ ) consisting of 70 mol%  $\text{Li}_4\text{SiO}_4$  and 30 mol%  $\text{Li}_2\text{TiO}_3$  were produced using the KALOS (Karlsruhe Lithium OrthoSilicate) process at Karlsruhe Institute of Technology, Karlsruhe, Germany [20]. The produced pebbles were thermally pre-treated at 900 °C for 3 weeks in air atmosphere using a muffle furnace in order to achieve an operation-relevant crystalline phase composition and microstructure. The crystalline phase composition was confirmed using both, powder X-ray diffractometry (p-XRD, D8 ADVANCE – Bruker AXS) and attenuated total reflection-Fourier transform infrared (ATR-FTIR) spectroscopy methods (VERTEX 70v – Bruker AXS). The thermally pre-treated pebbles consist of two main crystalline phases: monoclinic  $\text{Li}_4\text{SiO}_4$  and monoclinic  $\text{Li}_2\text{TiO}_3$  [2]. The pebbles may also contain negligible amounts of lithium hydroxide ( $\text{LiOH}$ ) and lithium carbonate ( $\text{Li}_2\text{CO}_3$ ), which can form on the pebble surface during handling, storage, and during measurement in air atmosphere [21]. The content of main constituents was determined using both, X-ray fluorescence (XRF, PIONEER S4 – Bruker AXS) and inductively coupled plasma optical emission spectrometry (ICP-OES, iCAP 7600 – ThermoFisher-Scientific) methods. Using XRF spectrometry, it was determined that the content of silicon is  $16.2 \pm 0.2$  wt% and that of titanium is  $12.20 \pm 0.09$  wt%. Using ICP-OES method, the determined content of main constituents has an excellent correlation with data obtained by XRF spectrometry:  $20.10 \pm 0.09$  wt% lithium,  $16.30 \pm 0.04$  wt% silicon, and  $11.90 \pm 0.02$  wt% titanium. Based on the determined content of silicon and titanium, the actual amount of  $\text{Li}_2\text{TiO}_3$  was evaluated using data from both methods: 30.6 mol% by XRF and 30.0 mol% by ICP-OES. The content of trace elements (impurities) was determined using only the ICP-OES method. The dominating metallic impurity is aluminium ( $0.0775 \pm 0.0008$  wt%), which is introduced in the pebbles during the production process by raw materials. The content of all other measured impurities is negligible, e.g., potassium ( $0.0067 \pm 0.0001$  wt%), calcium ( $0.0067 \pm 0.0001$  wt%), platinum ( $0.0061 \pm 0.0001$  wt%), iron ( $0.0057 \pm 0.0001$  wt%), gold ( $0.0030 \pm 0.0001$  wt%),

niobium ( $0.00286 \pm 0.00003$  wt%), magnesium ( $0.00211 \pm 0.00001$  wt%), sodium ( $0.00129 \pm 0.00003$  wt%), and zirconium ( $0.00119 \pm 0.00006$  wt%).

The irradiation experiments with X-rays were carried out using a custom-built setup equipped with an X-ray tube (tungsten anode, anode voltage: 45 kV, anode current: 10 mA, irradiation time: 30 min, room temperature, air atmosphere). The absorbed dose of the irradiated ACB pebbles is evaluated to be about 1 kGy. The low absorbed dose was selected in order to induce mainly the formation of primary radiation-induced defect centres due to trapping of mobile charge carriers (electrons and holes) created by the indirect ionisation on intrinsic defects (crystalline lattice imperfections) and extrinsic defects (impurity atoms) [17]. EPR spectroscopy investigations of the pebbles before and after irradiation were carried out with a Bruker ELEXSYS-II E500 spectrometer operated at the X microwave frequency band (9.82 GHz). For calibration of  $g$  value, a diphenyl-picrylhydrazyl (DPPH) reference sample ( $g = 2.0036$ ) was used. The spectra were acquired at room temperature in air atmosphere using 100 kHz magnetic field modulation frequency and 2 G modulation amplitude. To separate EPR signals with different power saturation characteristics, the microwave power was varied from 0.2 up to 200 mW. Other relevant EPR acquisition parameters were: sweep field width – 700 G; acquisition time – 70 s; number of scans – 4. The irradiated pebbles were stored at room temperature in air atmosphere for up to 35 days and EPR spectra were taken after certain time periods. To study the thermal stability of accumulated radiation-induced defect centres, the irradiated pebbles were isochronally annealed in air atmosphere using a custom-built furnace with an estimated temperature uncertainty of  $\pm 10$  °C. The annealing temperature was increased stepwise from room temperature up to 350 °C. The temperature interval between two annealing steps was 25 °C, while the dwell time of each annealing step was 10 min. After each annealing step, the pebbles were rapidly cooled down to room temperature for the EPR spectra measurements.

The stability tests of accumulated paramagnetic radiation-induced defect centres at room and elevated temperatures provided experimental data in order to identify and characterise individual signals contributing to the complex EPR spectra of the irradiated ACB pebbles. Afterwards, simulations of the experimental spectra as a superposition of several individual signals were performed using EasySpin software [22]. Solid-state EPR simulation functions *pepper* and *esfit* were used for the least-squares fitting procedure of the experimentally obtained spectra. Line broadenings were modelled using the *HStrain* function.

## 3. Results and discussion

EPR spectra dependence on microwave power for the ACB pebbles after irradiation with X-rays is shown in Fig. 1. No EPR signals were detected before the irradiation; therefore, the signals can be ascribed to radiation-induced defect centres. EPR spectra acquisition parameters were varied in order to analyse the contribution of individual paramagnetic radiation-induced defect centres. Three main groups of signals were detected with  $g$  values of about 2.04, 2.02–2.00, and 1.99–1.92. It is observed that the majority of signals scale with microwave power; however, for the signals in the  $g$  range of 2.02–2.00, variations in the line-shape are also evident. It has been demonstrated that the effect is caused by the presence of several overlapping EPR signals with different power-saturation characteristics [15,17].

EPR spectra simulations were performed to reconstruct the experimental spectrum as a superposition of several individual signals. In general, the principal  $g$  values in relation to the free-electron ( $g_e = 2.0023$ ) typically indicate whether the outer shell is more ( $g > g_e$ ) or less ( $g < g_e$ ) than half-filled [23]. Based on the shift from the  $g_e$  value, the analysis of experimental data is divided into two parts:  $g > 2.00$  range signals, which are typical for hole centres (HCs), and  $g < 2.00$  range signals, which can be assigned to electron centres (ECs). All signals were identified as spin  $S = \frac{1}{2}$  systems with no apparent hyperfine structure;

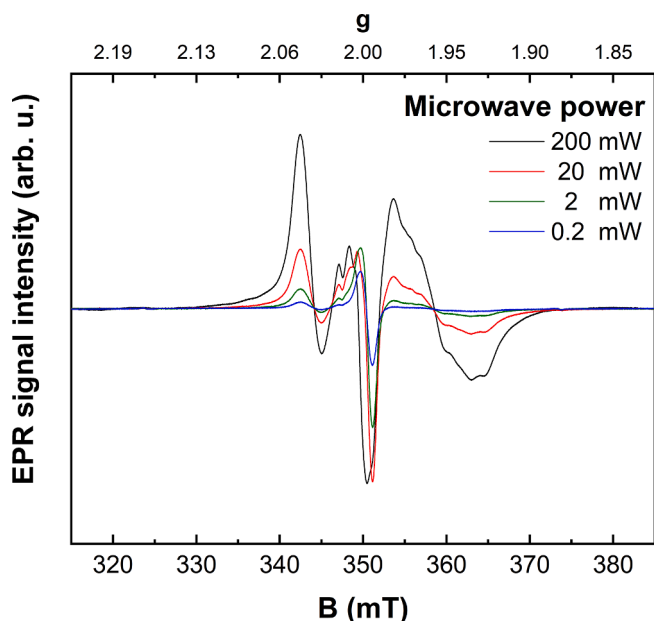


Fig. 1. EPR spectra of the ACB pebbles after irradiation with X-rays depending on microwave power.

therefore, the following SH was selected:

$$H = g\mu_B BS \quad (1)$$

where  $g$  is the  $g$ -factor;  $\mu_B$  – the Bohr magneton;  $B$  – external magnetic field;  $S$  – spin operator [24]. The following symmetries can be distinguished based on the principal values of the  $g$ -factor: isotropic ( $g_1 = g_2 = g_3$ ), axial ( $g_1 = g_2 \neq g_3$ ), and rhombic ( $g_1 \neq g_2 \neq g_3$ ).

The EPR simulation results for the  $g > 2.00$  range signals are presented in Fig. 2 and the determined SH parameters are summarised in Table 1. The spectrum acquired at 2 mW microwave power was selected for the analysis to minimise the contribution of  $g < 2.00$  range signals, but still provide a reasonable signal-to-noise ratio. All signals, apart from one rhombic symmetry signal, consist of a single symmetric line and can therefore be characterised by an isotropic  $g$  value. Previously, similar

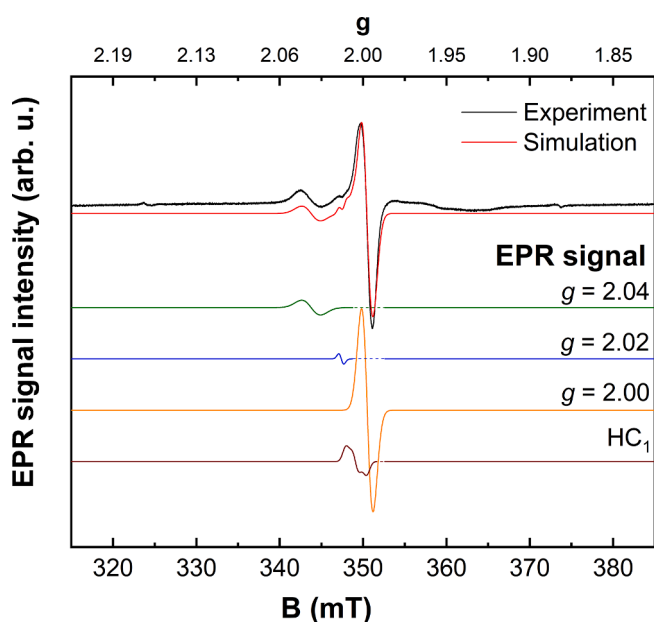


Fig. 2. Simulations of the experimental EPR spectrum (2 mW microwave power) as a superposition of individual signals in  $g > 2.00$  range.

Table 1

Determined SH parameters of individual EPR signals in  $g > 2.00$  range for paramagnetic radiation-induced defect centres in the irradiated ACB pebbles.

Designation	Symmetry	$g \pm 0.0010$
$g = 2.04$	Isotropic	2.0414
$g = 2.02$		2.0202
$g = 2.00$		2.0022
$HC_1$	Rhombic	2.0172 ( $g_1$ )
		2.0104 ( $g_2$ )
		2.0025 ( $g_3$ )

signals have been reported in irradiated single-phase  $Li_4SiO_4$  ceramic materials [25,26]. Therefore, the rhombic symmetry signal is attributed to the  $HC_1$  centre (hole trapped on a single non-bridging oxygen atom), and the determined principal components of the  $g$  tensor are in good agreement with multifrequency EPR analysis of the  $Li_4SiO_4$  pebbles produced with a surplus of  $SiO_2$  after irradiation with neutrons and photons of different types and energies [17]. However, an isotropic signal with  $g = 2.012$  attributed to the  $HC_2$  centre (hole delocalised over two non-bridging oxygen atoms bonded to the same silicon atom) is not detected in this case. The signal with  $g = 2.00$  could be attributed to  $E'$ -type centres (in the simplest case, an unpaired electron localised on a dangling tetrahedral ( $sp^3$ ) orbital of a single silicon atom) [27,28]. Presently, the origin of signal with  $g = 2.02$  is unknown. Previously, the signal with  $g = 2.04$  has been detected in the ACB pebbles after irradiation and could be attributed to various oxygen-related hole centres [14,18,21,29]. The signals of  $Li_2TiO_3$  as the second phase are not detected in this case due to the high radiation stability of this compound and relatively low absorbed dose [30]. Paramagnetic aluminium-related hole centres in quartz have also been reported to exhibit signals in this spectral range [27]; however, without the detection of characteristic  $^{27}Al$  hyperfine structure, definitive assignment, in this case, is problematic. As described previously, the content of other metallic impurities in the analysed pebbles is much smaller in comparison to aluminium impurities; therefore, the influence of these extrinsic defects on trapping of the created electrons and holes is highly unlikely. However, the possibility cannot be completely ruled out as the detection limits of commercial X-band EPR spectrometers can achieve sensitivities down to  $10^9$  spins per G linewidth [31].

The stability of the identified paramagnetic radiation-induced defect centres was investigated at room temperature; the results are shown in Fig. 3. The changes in EPR spectra shape at room temperature are related to decay or conversion reactions of unstable radiation-induced defect centres associated with shallow traps of mobile charge carriers (electrons or holes). Spectra recorded using 20 mW microwaves have been selected as representative for all of the detected signals (both  $g > 2.00$  and  $g < 2.00$  range). The signals with  $g = 2.04$ , 2.02 and 2.00 exhibit exponential decay. Nevertheless, the signals with  $g = 2.04$  and 2.02 are relatively more unstable in comparison to the signal with  $g = 2.00$ , which is in line with previous observations for the irradiated ACB pebbles [14,29]. EPR signal intensity of the  $HC_1$  centre shows a tendency to increase; however, it should be noted that the overlap with the dominant  $g = 2.00$  signal hinders unambiguous analysis. Signals with  $g < 2.00$  exhibit a complicated evolution with time, confirming the presence of multiple and overlapped anisotropic signals with similar  $g$  values.

A stepwise isochronal annealing experiment of the irradiated ACB pebbles was conducted to gain additional insights into the characteristics of the individual paramagnetic radiation-induced defect centres. The decrease of individual EPR signal intensities upon increasing the annealing temperature is caused by thermally stimulated recombination processes of the accumulated radiation-induced defect centres. As the annealing temperature is gradually increased, mobile charge carriers are detrapped from different trapping sites with various thermal activation energies, resulting in the decay of the corresponding EPR signals. The results, which are shown in Fig. 4, provide complementary information

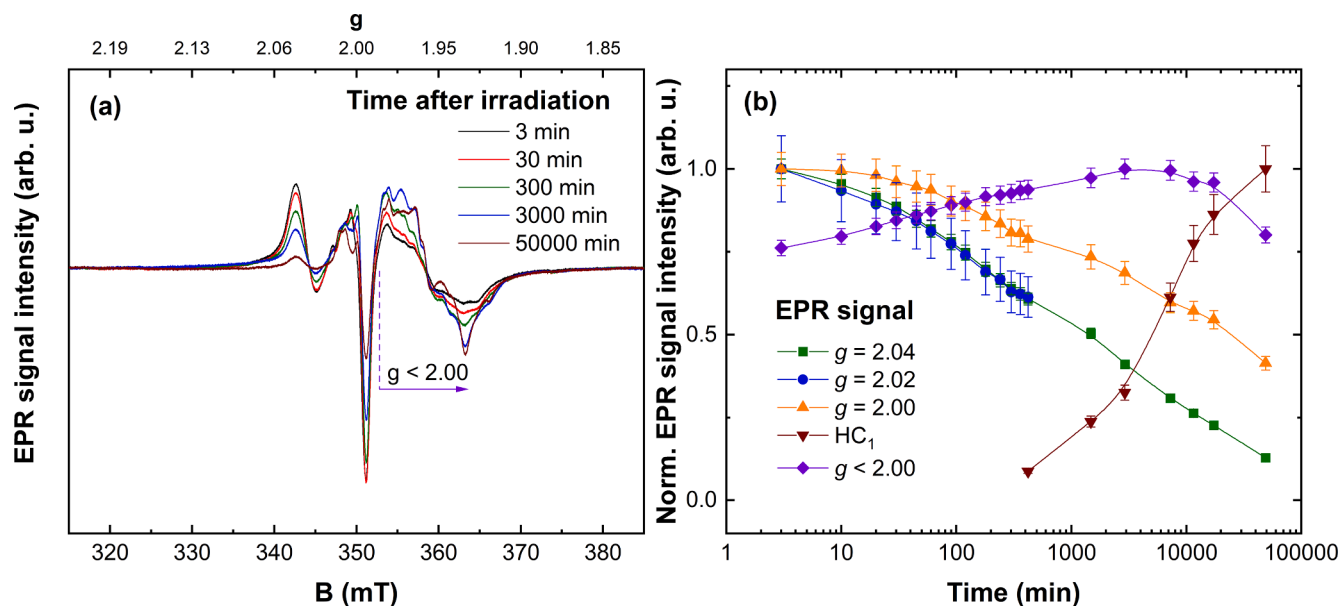


Fig. 3. (a) Evolution of EPR spectra (20 mW microwave power) and (b) stability of individual signals with time at room temperature.

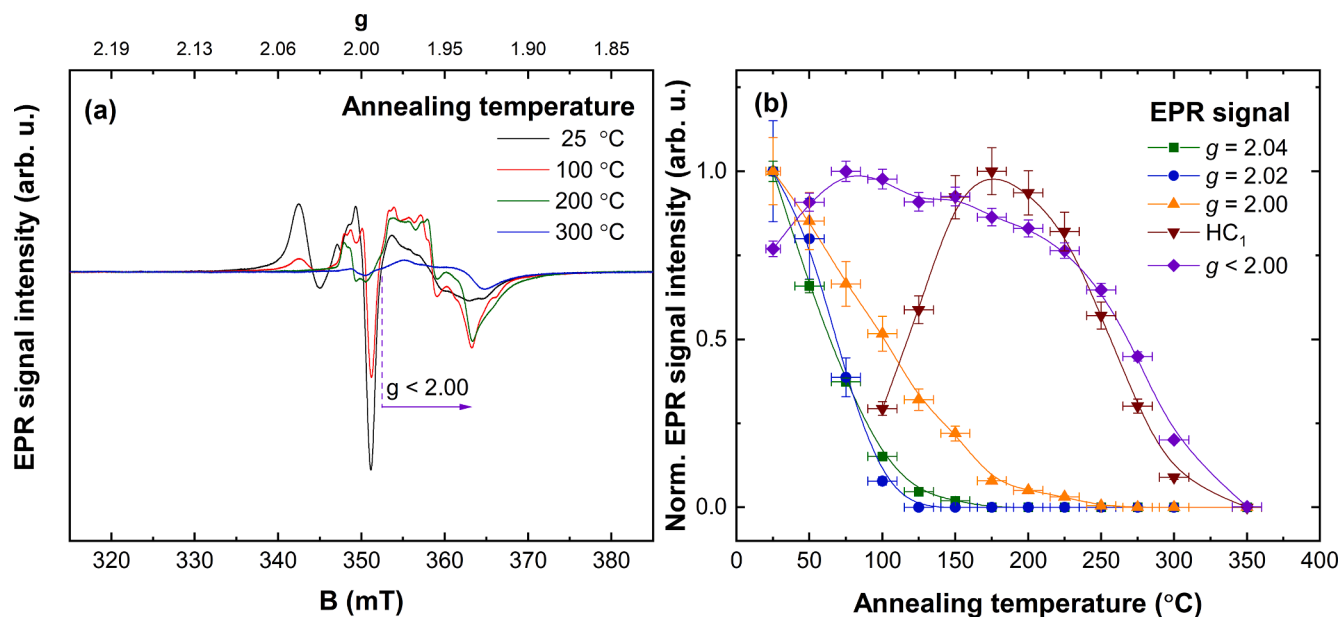


Fig. 4. (a) Evolution of EPR spectra (20 mW microwave power) and (b) stability of individual signals after sample annealing at different temperatures.

for Fig. 3 about the stability of accumulated radiation-induced defect centres at elevated temperature. As expected, EPR signal intensities of the least stable signals with  $g = 2.04$  and  $2.02$  decrease rapidly in the 25–100 °C annealing range. Annealing of the signal with  $g = 2.00$  can be divided into 25–150 and 175–250 °C intervals which differ by the rate of decay. The signal of the  $HC_1$  centre exhibits an initial increase, reaching maximum intensity after annealing in the 150–200 °C range, and a gradual decay onwards. The latter process is also correlated with the annihilation of signals with  $g < 2.00$ , which could be an indication of mutual recombination of the radiation-induced defect centres. The obtained results are also in good agreement with previous observations for the ACB pebbles under the simultaneous action of accelerated electrons and high temperature [18].

It is noteworthy to compare the obtained results with an analogous experiment performed on the irradiated  $Li_4SiO_4$  pebbles produced with a surplus of  $SiO_2$  [17]. Firstly, in the present work, the annealing curve

of the  $g = 2.00$  and  $HC_1$  signals is shifted by 25–50 °C towards higher temperatures, which exceeds the  $\pm 10$  °C margins of uncertainty of both experiments. Secondly, the signals with  $g < 2.00$  are formed only in the irradiated ACB pebbles. Therefore, it can be concluded that the addition of  $Li_2TiO_3$  as the second phase introduces additional electron traps, which stabilise other paramagnetic radiation-induced defect centres.

Detailed analysis of the EPR signals in  $g < 2.00$  range, which are related to ECs, is challenging, especially in the low-temperature annealing range, where the overlapping signals are broad and uninformative. However, some information, which is presented in Fig. 5 and Table 2, can be extracted from EPR spectra simulations after sample annealing above 150 °C. It was determined that, after annealing at 300 °C, the EPR spectrum can be ascribed to a single centre, further in text designated as EC(II), with nearly axially symmetric  $g$  tensor ( $g_2 \approx g_3$ ) and broad linewidths. When analysing the spectra for lower annealing temperatures, a contribution from a signal, further in text designated as

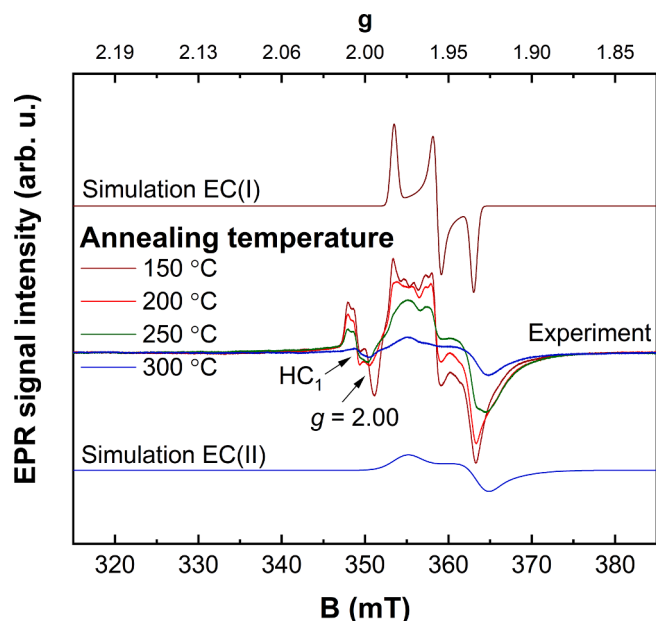


Fig. 5. Evolution of EPR spectra in the 150–300 °C annealing temperature range and simulations of individual signals in  $g < 2.00$  range.

Table 2

Determined SH parameters of individual EPR signals in  $g < 2.00$  range for paramagnetic radiation-induced defect centres in the irradiated ACB pebbles in the 150–300 °C annealing temperature range.

Designation	Symmetry	$g \pm 0.0010$
EC(I)	Rhombic	1.9854 ( $g_1$ )
		1.9568 ( $g_2$ )
		1.9330 ( $g_3$ )
EC(II)	Axial	1.9749 ( $g_1$ )
		1.9283 ( $g_2$ )
		1.9241 ( $g_3$ )

EC(I), is observed. The signal is composed of relatively narrow lines, which correspond to rhombic symmetry  $g$  tensor. Spectra evolution in the 150–300 °C annealing range suggests that the annealing of EC(I) is not a simple decay process but resembles a gradual EC(I)  $\rightarrow$  EC(II) transformation. It could be explained as if several radiation-induced defect centres with similar SH parameters, but different stabilities, are present or changes in the local structure of the paramagnetic centres occur.

The additions of  $\text{Li}_2\text{TiO}_3$  as the second phase must be considered to discuss the origin of several ECs in the irradiated ACB pebbles. Previously, no EPR signals in the  $g < 2.00$  range were detected in irradiated single-phase  $\text{Li}_4\text{SiO}_4$  or  $\text{Li}_2\text{TiO}_3$  ceramic materials [25,26]. Therefore, it can be concluded that  $\text{Li}_2\text{TiO}_3$  as the second phase introduces a variety of electron traps in the  $\text{Li}_4\text{SiO}_4$  phase, which form the detected paramagnetic radiation-induced defect centres after exposure to X-rays. Oxygen vacancies and other intrinsic and extrinsic defects are common electron traps in oxide materials [32]. Also, titanium-related electron centres are plausible candidates for  $S = \frac{1}{2}$  systems with different symmetries and  $g$  values presented in Table 2. It cannot be excluded that negligible amounts of titanium ions may be incorporated in the crystalline structure of the  $\text{Li}_4\text{SiO}_4$  phase during the production process. From previous studies, it is already known that the additions of polyvalent transition metal ions can significantly affect the formation of radiation-induced defect centres in single-phase  $\text{Li}_4\text{SiO}_4$  ceramic materials during irradiation [33,34]. During exposure to X-rays, electrons and holes are created by the indirect ionisation in the  $\text{Li}_4\text{SiO}_4$  phase of the ACB pebbles. Afterwards, the formed holes are trapped on intrinsic

defects, resulting in the formation of various HCs ( $\text{HC}_1$ , centres with  $g = 2.02$  and  $g = 2.04$  signals), while electrons could be trapped in oxygen vacancies (intrinsic defects), forming  $\text{E}'$ -type centres (possibly related to the  $g = 2.00$  signal), and on titanium impurities (extrinsic defects), resulting in the transformation of diamagnetic tetravalent titanium into paramagnetic trivalent titanium ( $\text{Ti}^{4+} \rightarrow \text{Ti}^{3+}$ ). However, the latter assignment has to be considered with caution because the detection of isolated  $\text{Ti}^{3+}$  centres by EPR is usually not feasible at room temperature and requires measurements at cryogenic temperatures [35–37]. To summarise, the formation of new types of paramagnetic radiation-induced defect centres, which modify thermal properties of the existing centres in the  $\text{Li}_4\text{SiO}_4$  phase, is stimulated in the ACB pebbles by adding  $\text{Li}_2\text{TiO}_3$  as the second phase.

#### 4. Conclusions

Multiple signals of spin  $S = \frac{1}{2}$  systems with distinctive symmetries and  $g$  values were identified and characterised in the ACB pebbles after irradiation with X-rays. It was determined that paramagnetic radiation-induced defect centres with EPR signals in the  $g > 2.00$  region are similar to irradiated single-phase  $\text{Li}_4\text{SiO}_4$  ceramic materials, while additions of  $\text{Li}_2\text{TiO}_3$  as the second phase in the ACB pebbles also stimulates the formation of several titanium-related electron centres with signals in the  $g < 2.00$  region. The signals with  $g = 2.04$ ,  $2.02$  and  $2.00$  are unstable at room temperature and exhibit exponential decay over time. However, the annealing of several radiation-induced defect centres is shifted by 25–50 °C towards higher temperatures in comparison to the irradiated  $\text{Li}_4\text{SiO}_4$  pebbles produced with a surplus of  $\text{SiO}_2$ , suggesting the stabilisation of paramagnetic centres in the ACB pebbles. In addition, after annealing in the 150–300 °C temperature range, a complex evolution of EPR signals with  $g < 2.00$  assigned to titanium-related electron centres was observed, which could be attributed to changes in the local structure of the respective radiation-induced defect centres.

#### CRedit authorship contribution statement

**Arturs Zarins:** Conceptualization, Methodology, Validation, Formal analysis, Investigation, Writing – original draft, Writing – review & editing, Visualization, Funding acquisition. **Andris Antuzevics:** Conceptualization, Methodology, Validation, Formal analysis, Investigation, Writing – original draft, Writing – review & editing, Visualization. **Gunta Kizane:** Conceptualization, Writing – review & editing, Resources, Supervision, Project administration. **Julia M. Leys:** Conceptualization, Resources, Writing – review & editing. **Regina Knitter:** Conceptualization, Resources, Writing – review & editing.

#### Declaration of Competing Interest

The authors declare that they have no known competing financial interests or personal relationships that could have appeared to influence the work reported in this paper.

#### Data availability

Data will be made available on request.

#### Acknowledgements

This study has been performed within the framework of European Regional Development Fund (ERDF) project (application No. 1.1.1.2/VIAA/4/20/614). Institute of Solid State Physics, University of Latvia as the Center of Excellence has received funding from the European Union's Horizon 2020 Framework Programme H2020-WIDESPREAD-01-2016-2017-TeamingPhase2 under grant agreement No. 739508, project CAMART2.

## References

- [1] A. Becoulet, ITER team. Progress on ITER construction and engineering. *Fusion Engineering and Design*, 188 (2023) 113424. 10.1016/j.fusengdes.2023.113424.
- [2] R. Knitter, M.H.H. Kolb, U. Kaufmann, A.A. Goraieb, Fabrication of modified lithium orthosilicate pebbles by addition of titania, *J. Nucl. Mater.* 442 (2013) s433–s436, <https://doi.org/10.1016/j.jnucmat.2012.10.034>.
- [3] M. Zmitko, P. Vladimirov, R. Knitter, M. Kolb, O. Leys, J. Heuser, H.-C. Schneider, R. Rolli, V. Chakin, S. Pupleschi, L. Magielsens, A. Fedorov, Y. Poitevin, Development and qualification of functional materials for the European HCPB TBM, *Fusion Eng. Des.* 136 (2018) 1376–1385, <https://doi.org/10.1016/j.fusengdes.2018.05.014>.
- [4] O. Leys, J.M. Leys, R. Knitter, Current status and future perspectives of EU ceramic breeder development, *Fusion Eng. Des.* 164 (2021), 112171, <https://doi.org/10.1016/j.fusengdes.2020.112171>.
- [5] F.A. Hernández, F. Arbeiter, L.V. Boccaccini, E. Bubelis, V.P. Chakin, I. Cristescu, B. E. Ghidersa, M. González, W. Hering, M. Hernández, X.Z. Jin, M. Kamlah, B. Kiss, R. Knitter, M.H.H. Kolb, P. Kurinskiy, O. Leys, I.A. Maione, M. Moscardini, G. Nádas, H. Neuberger, P. Pereslavtsev, S. Pupleschi, R. Rolli, S. Ruck, G. A. Spagnuolo, P.V. Vladimirov, C. Zeile, G. Zhou, Overview of the HCPB Research Activities in EUROfusion, *IEEE Trans. Plasma Sci.* 46 (2018) 2247–2261, <https://doi.org/10.1109/TPS.2018.2830813>.
- [6] M.H.H. Kolb, R. Knitter, T. Hoshino,  $\text{Li}_2\text{SiO}_4$  based breeder ceramics with  $\text{Li}_2\text{TiO}_3$ ,  $\text{LiAlO}_2$  and  $\text{Li}_x\text{La}_y\text{TiO}_3$  additions, part II: Pebble properties, *Fusion Eng. Des.* 115 (2017) 6–16, <https://doi.org/10.1016/j.fusengdes.2016.12.038>.
- [7] D.A.H. Hanaor, M.H.H. Kolb, Y. Gan, M. Kamlah, R. Knitter, Solution based synthesis of mixed-phase materials in the  $\text{Li}_2\text{TiO}_3$ – $\text{Li}_4\text{SiO}_4$  system, *J. Nucl. Mater.* 456 (2015) 151–161, <https://doi.org/10.1016/j.jnucmat.2014.09.028>.
- [8] J.M. Heuser, M.H.H. Kolb, T. Bergfeldt, R. Knitter, Long-term thermal stability of two-phased lithium orthosilicate/metatitanate ceramics, *J. Nucl. Mater.* 507 (2018) 396–402, <https://doi.org/10.1016/j.jnucmat.2018.05.010>.
- [9] M.H.H. Kolb, R. Rolli, R. Knitter, Tritium adsorption/release behaviour of advanced EU breeder pebbles, *J. Nucl. Mater.* 489 (2017) 229–235, <https://doi.org/10.1016/j.jnucmat.2017.03.051>.
- [10] K. Mukai, P. Pereslavtsev, U. Fischer, R. Knitter, Activation calculations for multiple recycling of breeder ceramics by melt processing, *Fusion Eng. Des.* 100 (2015) 565–570, <https://doi.org/10.1016/j.fusengdes.2015.08.007>.
- [11] A. Zarins, O. Leys, G. Kizane, A. Supe, L. Baumane, M. Gonzalez, V. Correcher, C. Boronat, A. Zolotarjovs, R. Knitter, Behaviour of advanced tritium breeder pebbles under simultaneous action of accelerated electrons and high temperature, *Fusion Eng. Des.* 121 (2017) 167–173, <https://doi.org/10.1016/j.fusengdes.2017.06.033>.
- [12] K. Mukai, F. Sanchez, R. Knitter, Chemical compatibility study between ceramic breeder and EUROFER97 steel for HCPB-DEMO blanket, *J. Nucl. Mater.* 488 (2017) 196–203, <https://doi.org/10.1016/j.jnucmat.2017.03.018>.
- [13] S.K. Misra, *Multifrequency Electron Paramagnetic Resonance: Theory and Applications*, Wiley (2011), <https://doi.org/10.1002/9783527633531>.
- [14] J. Cipa, A. Zarins, A. Supe, G. Kizane, A. Zolotarjovs, L. Baumane, L. Trinkler, O. Leys, R. Knitter, X-ray induced defects in advanced lithium orthosilicate pebbles with additions of lithium metatitanate. *Fusion Engineering and Design*, 143 (2019) 10–15. 10.1016/j.fusengdes.2019.03.096.
- [15] J.M. Leys, A. Zarins, J. Cipa, L. Baumane, G. Kizane, R. Knitter, Radiation-induced effects in neutron- and electron-irradiated lithium silicate ceramic breeder pebbles, *J. Nucl. Mater.* 540 (2020), 152347, <https://doi.org/10.1016/j.jnucmat.2020.152347>.
- [16] H. Ishikawa, T. Suda, A. Yoshikawa, M. Oyaidzu, K. Ochiai, C. Konno, K. Munakata, Y. Oya, K. Okuno. Study on correlation between tritium release behavior and annihilation behavior of irradiation defects in neutron-irradiated  $\text{Li}_4\text{SiO}_4$ . *Fusion Science and Technology*, 54 (2017) 127–130. 10.13182/FST08-A1779.
- [17] A. Antuzevics, A. Zarins, A. Anson, J. Cipa, G. Kizane, J.M. Leys, R. Knitter, Thermal properties of paramagnetic radiation-induced defects in lithium orthosilicate containing breeder material, *J. Nucl. Mater.* 565 (2022), 153713, <https://doi.org/10.1016/j.jnucmat.2022.153713>.
- [18] A. Zarins, O. Valtensbergs, G. Kizane, A. Supe, R. Knitter, M.H.H. Kolb, O. Leys, L. Baumane, D. Conka, Formation and accumulation of radiation-induced defects and radiolysis products in modified lithium orthosilicate pebbles with additions of titanium dioxide, *J. Nucl. Mater.* 470 (2016) 187–196, <https://doi.org/10.1016/j.jnucmat.2015.12.027>.
- [19] I. Kenzhina, T. Kulsartov, R. Knitter, Y. Chikhray, Y. Kenzhin, Z. Zaurbekova, A. Shaimerdenov, G. Kizane, A. Zarins, A. Kozlovskiy, M. Gabdullin, A. Tolenova, E. Nesterov, Analysis of the reactor experiments results on the study of gas evolution from two-phase  $\text{Li}_2\text{TiO}_3$ – $\text{Li}_4\text{SiO}_4$  lithium ceramics, *Nuclear Materials and Energy* 30 (2022), 101132, <https://doi.org/10.1016/j.nme.2022.101132>.
- [20] O. Leys, T. Bergfeldt, M.H.H. Kolb, R. Knitter, A.A. Goraieb, The reprocessing of advanced mixed lithium orthosilicate/metatitanate tritium breeder pebbles, *Fusion Eng. Des.* 107 (2016) 70–74, <https://doi.org/10.1016/j.fusengdes.2016.04.025>.
- [21] A. Zarins, O. Valtensbergs, G. Kizane, A. Supe, S. Tamulevicius, M. Andrulevicius, E. Pajuste, L. Baumane, O. Leys, M.H.H. Kolb, R. Knitter, Characterisation and radiolysis of modified lithium orthosilicate pebbles with noble metal impurities, *Fusion Eng. Des.* 124 (2017) 934–939, <https://doi.org/10.1016/j.fusengdes.2017.01.008>.
- [22] S. Stoll, A. Schweiger, EasySpin, a comprehensive software package for spectral simulation and analysis in EPR, *J. Magn. Reson.* 178 (2006) 42–55, <https://doi.org/10.1016/j.jmr.2005.08.013>.
- [23] V. Jary, L. Havlak, J. Barta, E. Mihokova, R. Kucerkova, M. Buryi, V. Babin, P. Prusa, T. Vrba, A. Kotlov, M. Nikl, Efficient Ultrafast Scintillation of  $\text{KLu}_2\text{Pr}^{3+}$  Phosphor: A Candidate for Fast-Timing Applications, *Phys. Rev. Appl.* 19 (2023), 034092, <https://doi.org/10.1103/PhysRevApplied.19.034092>.
- [24] J.A. Weil, J.R. Bolton, *Electron Paramagnetic Resonance*, Wiley, 2007.
- [25] B. Ji, S. Gu, Q. Qi, X.-C. Li, Y. Zhang, H. Zhou, G.N. Luo, Annihilation kinetics of irradiation defects in promising tritium breeding pebbles, *Nuclear Materials and Energy* 27 (2021), 101015, <https://doi.org/10.1016/j.nme.2021.101015>.
- [26] G. Ran, C. Xiao, X. Chen, Y. Gong, L. Zhao, H. Wang, X. Wang, Annihilation behavior of irradiation defects in  $\text{Li}_4\text{SiO}_4$  irradiated with high thermal neutron fluence, *J. Nucl. Mater.* 491 (2017) 43–47, <https://doi.org/10.1016/j.jnucmat.2017.04.055>.
- [27] R.I. Mashkovtsev, Y. Pan. Nature of paramagnetic defects in  $\alpha$ -quartz: Progresses in the first decade of the 21st century, in: *New Developments in Quartz Research: Varieties, Crystal Chemistry and Uses in Technology*, 2013: pp. 65–104.
- [28] A. Alessi, S. Agnello, G. Buscarino, Y. Pan, R.I. Mashkovtsev. EPR on radiation-induced defects in  $\text{SiO}_2$ , in: *Applications of EPR in Radiation Research*, 2014: pp. 255–295. 10.1007/978-3-319-09216-4\_7.
- [29] J.M. Heuser, A. Zarins, L. Baumane, G. Kizane, R. Knitter, Radiation stability of long-term annealed bi-phasic advanced ceramic breeder pebbles, *Fusion Eng. Des.* 138 (2019) 395–399, <https://doi.org/10.1016/j.fusengdes.2018.12.034>.
- [30] J. Tiliks, G. Kizane, A. Vitins, G. Vitins, J. Meisters, Physicochemical processes in blanket ceramic materials, *Fusion Eng. Des.* 69 (2003) 519–522, [https://doi.org/10.1016/S0920-3796\(03\)00120-0](https://doi.org/10.1016/S0920-3796(03)00120-0).
- [31] G.R. Eaton, S.S. Eaton, D.P. Barr, R.T. Weber, *Quantitative EPR*, Springer, 2010.
- [32] M. Nikl, V.V. Laguta, A. Vedda. Complex oxide scintillators: Material defects and scintillation performance. *Physica Status Solidi (B) Basic Research*, 245 (2008) 1701–1722. 10.1002/pssb.200844039.
- [33] J.E. Tiliks, G.K. Kizane, A.A. Supe, A.A. Abramkovs, J.J. Tiliks, V.G. Vasiljev, Formation and properties of radiation-induced defects and radiolysis products in lithium orthosilicate, *Fusion Eng. Des.* 17 (1991) 17–20, [https://doi.org/10.1016/0920-3796\(91\)90029-P](https://doi.org/10.1016/0920-3796(91)90029-P).
- [34] A. Abramkovs, J. Tiliks, G. Kizane, V. Grishmanovs, A. Supe, Basic study of influence of radiation defects on tritium release processes from lithium silicates, *J. Nucl. Mater.* 248 (1997) 116–120, [https://doi.org/10.1016/S0022-3115\(97\)00206-7](https://doi.org/10.1016/S0022-3115(97)00206-7).
- [35] S.A. Al'tshulter, B.M. Kozyrev, *Electron Paramagnetic Resonance in Compounds of Transition Elements*, Wiley, 1974.
- [36] E.Y. Wong, Paramagnetic resonance of  $\text{Ti}^{3+}$ ,  $\text{Cr}^{3+}$ , and  $\text{Fe}^{3+}$  in  $\text{AlCl}_3 \cdot 6\text{H}_2\text{O}$ , *J. Chem. Phys.* 32 (1960) 598–600, <https://doi.org/10.1063/1.1730742>.
- [37] H. Rinneberg, J.A. Weil, EPR studies of  $\text{Ti}^{3+}$ – $\text{H}^+$  centers in x-irradiated  $\alpha$ -quartz, *J. Chem. Phys.* 56 (1972) 2019–2028, <https://doi.org/10.1063/1.1677493>.